Development of white matter tracts between and within the dorsal and ventral streams

Abbreviated title: Dorsal-ventral white matter development

Authors' Names: Vinci-Booher, S.*[1], Caron, B.[1], Bullock, D.[1], James, K.[1], & Pestilli, F.*[1,2]

Author Affiliations: [1]Indiana University, Bloomington, Indiana, USA; [2]University of Texas, Austin, Texas, USA

***Corresponding Authors:**

Franco Pestilli
Department of Psychology
The University of Texas at Austin
108 E Dean Keeton St, Austin, TX 78712
(347) 829- 4185, pestilli@utexas.edu

Sophia Vinci-Booher
Department of Psychological and Brain Sciences
Indiana University
1101 E. 10th Street, Bloomington, IN 47405
(812) 855-1494, svincibo@indiana.edu

Acknowledgments

This research was funded by NSF OAC-1916518, NSF IIS-1912270, NSF IIS-1636893, NSF BCS-1734853, Microsoft Investigator Fellowship to F.P. Data collections as supported by The Emergent Areas or Research Indiana University to F. Pestilli, K. James, and L. Smith, the Indiana University Bloomington Imaging Research Facility Brain Scan Credit Program, the Indiana Clinical and Translational Sciences Institute, and the Johnson Center for Innovation and Translational Research provided additional imaging funds. SVB was partially supported by the NIH T32-HD007475-21 and the EAR Initiative Linda Smith (Indiana University). DNB was partially supported by NIH NIMH T32-MH103213 to William Hetrick (Indiana University). The authors would like to acknowledge the help of Dr. Hu Cheng for help with the imaging sequences, Soichi Hayashi and Brent McPherson for contributing to the development of brainlife.io.

Author Contribution Statement

Sophia Vinci-Booher contributed to all aspects of the manuscript, including the original conception of the study, ongoing conceptual development, the design, data collection, analyses and software, writing the original draft of the paper, and revisions. Brad Caron and Dan Bullock contributed software and supported software development, participated in data quality checks, and commented on the manuscript. Karin James contributed to data collection and commented on the manuscript. Franco Pestilli contributed to the conceptual development of the work, the design, the analyses, software, training, and the writing of the manuscript.

Conflict of Interest Statement

The authors declare no competing financial interests.

Abstract
The degree of interaction between the ventral and dorsal visual streams has been discussed in multiple scientific domains for decades. Recently, several white matter tracts that directly connect the dorsal and ventral streams have become possible to study using automated and reproducible methods. The developmental trajectory of this set of tracts, the posterior vertical pathway (PVP), is yet to be described. We propose an input-driven model of white matter development and provide evidence for the model by focusing on PVP development. We used reproducible cloud-computing methods and diffusion imaging from adults and children (ages 5-8 years) to compare PVP development to that of tracts within the ventral and dorsal pathways. PVP microstructure was more adult-like than dorsal stream microstructure but less adult-like than ventral stream microstructure. Additionally, PVP microstructure was more similar to the microstructure of the ventral than dorsal stream and was predicted by performance on a perceptual task in children. Overall, results suggest a key role for the PVP in the development of the dorsal visual stream that may be related to its ability to facilitate interactions between ventral and dorsal streams during learning. The results are consistent with the proposed model, suggesting that the microstructural development of major white matter pathways is related, at least in part, to the feed-forward propagation of sensory information within the visual system.

Significance Statement
Understanding white matter development is important to building predictive models that can inform interventions and targeted educational methods. We propose and provide evidence for an input-driven model of white matter development. We tested an uncharted aspect of human brain development. Namely, how the recently described posterior vertical white matter tracts develop. Our results suggest a feed-forward developmental progression along the known direct anatomical connections from posterior visual areas to anterior ventral and dorsal areas. Our results suggest fundamental biological mechanisms that clarify the role of white matter in predicting human learning and behavior.

Introduction
Visual information in the human brain is processed along two processing streams, the dorsal and ventral streams (1–7). A large body of work has demonstrated a degree of functional segregation between perceptual processing associated with the ventral stream and action processing associated with the dorsal stream (1, 2, 6, 8–11). However, these two streams do interact (5, 7, 12, 13) and a handful of studies suggest that the two streams interact differently in childhood than in adulthood (14, 15).

Recent work has reported a set of vertical white matter tracts that directly connect cortical regions associated with ventral and dorsal streams (3, 16–25). We refer to this collection of white matter tracts as the Posterior Vertical Pathway (PVP; see **Figure 1a**). The PVP comprises four tracts for which automated segmentation algorithms have only recently been made available (25). Two of these tracts connect posterior ventral temporal cortex to either inferior parietal cortex (i.e., posterior Arcuate, pArc) or superior parietal cortex (i.e., Temporal Parietal connection to the Superior Parietal Lobe, TP-SPL), while the other two tracts connect anterior ventral temporal cortex to either inferior parietal cortex (i.e., Middle Longitudinal Fasciculus to the Angular Gyrus, MDLFang) or superior parietal cortex (i.e., Middle

Longitudinal Fasciculus to the Superior Parietal Lobe, MDLFspl). Understanding the development of the PVP can help clarify the mechanisms underlying interactions between the dorsal and ventral streams in childhood and in adulthood.

As of today, only a handful of studies have investigated the development of tracts within the PVP. With the exception of a few studies reporting correlations between the pArc and behavior (26–32), most prior work has focused almost exclusively on horizontal white matter tracts contained *within* the ventral or dorsal streams (33–40). Consequently, we know very little about the development of PVP tracts that support the transfer of information *between* the ventral and dorsal streams. Furthermore, prior work has employed a tract-of-interest approach, studying the developmental trajectory of individual tracts instead of the developmental relationships among tracts. Consequently, we know very little about the relative development of ventral, dorsal, and PVP white matter tracts. More specifically, we do not know how the development of the PVP may be related to and may contribute to the development of the ventral and dorsal streams. Our goal was to fill these gaps: (1) the paucity of studies concerning the development of tracts within the PVP and (2) the developmental relationships among the PVP and ventral and dorsal streams. Filling these gaps can provide insight into the mechanisms underlying white matter development as well as mechanisms of interaction between dorsal and ventral streams.

Materials and Methods

Participants

Children and adult participants were recruited for this study. Children (5-8 yrs., n = 50) were recruited through an in-house database of parents in the local community who had expressed interest in participating in developmental psychological research and through word-of-mouth. Literate adult participants (18-25 yrs., n = 17) were recruited through an in-house database of IU students who had expressed interest in participating in psychological research at IU and through word-of-mouth. Of these, we obtained diffusion data from 31 children and 13 adults. Additional participant diffusion data were removed based on signal-to-noise (SNR) and/or motion concerns, leaving 24 children (age: M = 6.7 years, SD = 1.3 years, Range = [4.7, 8.4], 15F, 9M) and 12 adults (age: M = 20.1 years, SD = 0.9 years, Range = [18.3, 21.2], 6F, 6M).

All participants were screened for neurological trauma, developmental disorders, and MRI contraindications. All participants were right-handed with English as their native language. Child participants were compensated with a small toy or gift card. Adult participants were compensated with a gift card.

Behavioral Assessment

Children completed a behavioral session consisting of a battery of standard assessments designed to assess visual-motor integration (Beery VMI: green, blue, and brown; 113), fine motor skill (Grooved Pegboard; 114, 115), and literacy level (WJ-IV Achievement: Letter-Word Identification, Spelling, Word Attack, Spelling of Sounds; 116). Assessments were administered in the same order for all participants.

Raw scores for the Grooved Pegboard were measured in seconds to completion. All other raw scores were measured as the number of correct items.

A composite score quantified the abilities of each participant on three dimensions: visual-motor skill, fine motor skill, and literacy. The visual-motor composite score (VM) was calculated by averaging the percentage of correct responses on the Beery Visual-Motor Integration, Beery Visual Perception, and Beery Motor Coordination assessments. The fine motor skill composite score (FM) was calculated by averaging the time taken on the Grooved Pegboard for both hands, dividing by the number of rows completed (i.e., the children only complete two rows whereas the adults complete five rows), taking the inverse to make higher scores correspond to higher skill, and, finally, multiplying by one hundred to scale the score. The literacy composite score (LIT) was calculated by averaging the percentage of correct responses on the Woodcock Johnson IV Letter-Word Identification, WJ-IV Spelling, WJ-IV Word Attack, and WJ-IV Spelling of Sounds. Group means and standard deviations for the behavioral measures and composite scores are reported in **Table 1**.

Table 1 Descriptive Statistics and Behavioral Measures

	Age Group	
	Children (n=24)	Adults (*n* = 12)
	M (SD)	*M* (*SD*)
Age (years)	6.7 (1.3)	20.1 (0.9)
Beery		
Visual-Motor Integration	18.3 (3.6)	27.1 (1.9)
Visual Perception	20.9 (3.9)	27.2 (2.6)
Motor Coordination	18.1 (3.9)	25.2 (2.6)
Grooved Pegboard		
Dominant hand (right)	42.4 (14.0)	61.1 (8.5)
Non-dominant hand (left)	45.7 (17.8)	62.8 (6.2)
Woodcock Johnson IV		
Letter Word Identification	37.4 (21.0)	70.5 (3.1)
Spelling	17.3 (9.8)	46.7 (4.3)
Word Attack	15.8 (7.8)	33.1 (21.8)
Spelling of Sounds	11.1 (6.2)	25.8 (2.9)
Composite Scores		
Visual Motor	19.1 (3.1)	26.5 (1.3)
Fine Motor	5.0 (1.5)	3.3 (0.3)
Literacy	20.4 (10.8)	44.0 (6.5)

Behavioral testing occurred within 3 weeks of the neuroimaging session. Grooved Pegboard is reported in seconds to completion. All others are reported in a number of correct items. Composite scores were calculated by combining scores on more than one assessment, as reported in the main text.

Imaging Procedure

Child participants were first acclimated to the MRI environment by practice sessions in a full-sized and fully-equipped mock MRI scanner. Children who completed the mock training session with success and

comfort were then escorted into the MRI environment. Adult participants skipped the mock training session. All participants wore ear protection in the MRI. All participants wore a Wheaton® elastic shoulder immobilizer to reduce motion. When space allowed, we used an inflatable head immobilization padding in the head coil. Participants were allowed to watch a movie, listen to an audio book, or to simply rest. Participants that successfully completed the neuroimaging session were asked to complete an additional behavioral session within one week of the neuroimaging session.

Magnetic Resonance Image Acquisition

Neuroimaging was performed at the Indiana University Imaging Research Facility, housed within the Department of Psychological and Brain Sciences with a 3-Tesla Siemens Prisma whole-body MRI using a 32-channel head coil. High-resolution T1-weighted anatomical volumes were acquired using a Turbo-flash 3-D sequence: TI = 900 ms, TE = 2.7 ms, TR = 1800 ms, flip angle = 9°, with 160 sagittal slices of 1.0 mm thickness, a field of view of 256 x 256 mm, and an isometric voxel size of 1.0 mm^3. Total acquisition time was 5 minutes and 12 seconds.

Diffusion data were collected using single-shot spin echo simultaneous multi-slice (SMS) EPI (transverse orientation, TE = 83.60 ms, TR = 3495 ms, flip angle = 90 degrees, isotropic 1.5 mm resolution; FOV = LR 210 mm x 192 mm x 138 mm; acquisition matrix MxP = 140 x 128. SMS acceleration factor = 4). Data collected in the AP fold-over direction were collected at two diffusion gradient strengths, with 38 diffusion directions at b = 1,000 s/mm^2 and 37 directions at b = 2,500 s/mm^2. We then collected 10 diffusion images at b = 0 s/mm^2 in the PA phase-encoding direction to use for distortion corrections. The total acquisition time was approximately 6 minutes.

Magnetic Resonance Imaging Data Analyses

All analysis steps were performed using open and reproducible cloud services on the brainlife.io platform (74) except for the statistical analyses that were performed in Matlab R2019b using customized code. All data and code are freely available on brainlife.io and/or github.com (**Table 2**).

Application	Github repository	Open Service DOI	Git Branch
HCP AC-PC Alignment	https://github.com/brain-life/app-hcp-acpc-alignment	doi.org/10.25663/bl.app.99	1.4
Freesurfer Segmentation	https://github.com/brainlife/app-freesurfer	doi.org/10.25663/bl.app.0	1.7
Distortion and motion Correction	https://brainlife.io/app/5e6e72838a20890d8a8e96af	doi.org/10.25663/brainlife.app.287	master
dMRI Preprocessing	https://github.com/brain-life/app-mrtrix3-preproc	doi.org/10.25663/bl.app.68	1.5
Tractography	https://github.com/brain-life/app-mrtrix3-act	doi.org/10.25663/bl.app.101	1.3
Tract Segmentation	https://github.com/brainlife/app-wmaSeg	doi.org/10.25663/brainlife.app.188	3.3
Tract Cleaning	https://github.com/brainlife/app-removeTractOutliers	doi.org/10.25663/brainlife.app.195	1.3
Tract Analysis Profiles	https://github.com/brain-life/app-tractanalysisprofiles	doi.org/10.25663/brainlife.app.185	1.8
Tract Statistics	https://github.com/brainlife/app-tractographyQualityCheck	doi.org/10.25663/brainlife.app.189	1.2

Table 2. Data, description of analyses, and web-links to the open source code and open cloud services used in the creation of this dataset can be viewed in their entirety here: https://doi.org/10.25663/brainlife.pub.15.

Anatomical (T1w) processing. Anatomical images were aligned to the AC-PC plane with an affine transformation using HCP preprocessing pipeline (117) as implemented in the HCP AC-PC Alignment App on brainlife.io (75). Images from child subjects were aligned using a pediatric atlas created from 5-8 year old children (118); images from adult subjects were aligned to the standard MNI152 adult template (117). AC-PC aligned images were then segmented using the Freesurfer 6.0 (119) as implemented in the Freesurfer App on brainlife.io (120) to generate the cortical volume maps with labeled cortical regions according to the Destrieux 2009 atlas (121).

Diffusion (dMRI) processing. AP phase-encoded and PA phase-encoded images were combined using FSL Topup & Eddy with customized lambda values (122). Susceptibility- and eddy current-induced distortions as well as inter-volume subject motion were also corrected in this step. All other diffusion preprocessing steps were then performed using the recommended mrtrix3 preprocessing steps (123) as implemented in the Mrtrix3 Preprocess App on brainlife.io (76). PCA denoising and Gibbs deringing procedures were performed first. The volumes were then corrected for bias field and rician noise. Finally, the preprocessed dMRI data and gradients were aligned to each participant's ACPC-aligned anatomical image using boundary-based registration (BBR) in FSL (124).

White matter measurements. The microstructural properties of white matter tissue were estimated in a voxel-wise fashion based on preprocessed dMRI data. We measured fractional anisotropy (FA) by fitting the diffusion tensor model on single-shell data (77, 78). FA is a summary measure of tissue microstructure that is related to white matter integrity and has been demonstrated to be reliable across a wide age range (37).

Tractography. Probabilistic tractography (PT) was used to generate streamlines. We used constrained spherical deconvolution (CSD) to model the diffusion tensor for tracking (125, 126). Tracking with the CSD model fit was performed probabilistically using the tractography procedures provided by Mrtrix3 Anatomically-constrained Tractography (ACT; 127, 128) implemented in brainlife.io (78). We generated 2 million streamlines at L_{max} = 8 and maximum curvatures = 35 degrees. The tractogram was then segmented using a recently developed segmentation approach (25) implemented in brailife.io (79) that uses a method similar to white matter query language (WMQL; 129, 130).

Cleaning. Streamlines that were shorter than 10 mm or longer than 200 mm were excluded. Streamlines that were more than 4 standard deviations away from the centroid of each tract and/or 4 standard deviations away from the tract's average streamline length were considered aberrant streamlines and were removed using the Remove Tract Outliers App on brainlife.io (131).

Tract profiles. Tract-profiles were generated for each major tract (39) as well as the additional PVP tracts (25) using the Tract Analysis Profiles app on brainlife.io (80). We first segmented each streamline

in a particular tract into 200 equally-spaced nodes. At each node, we estimated the location of the tract's 'core' by averaging the x, y, and z coordinates of each streamline at that node. We then estimated FA at each node of the core by averaging across streamlines within that node weighted by the distance of the streamline from the 'core' (**Figure 2b**). Averages for each tract were calculated by averaging across the central 160 nodes, excluding the first and last 20 nodes to avoid partial voluming effects. Group averages for each tract were calculated by averaging the tract average within each group.

Experimental Design and Statistical Analysis

We assessed differences in the developmental trajectory among white matter pathways (i.e., VOF, VHP, PVP, DHP, FAT) based on how adult-like these white matter pathways were in our child sample. We operationalized 'adult-like' as the difference in the average microstructural measurement of a tract between children and adults, similar to other works (33, 36, 40). A smaller difference would suggest that the pathway is more adult-like than a pathway with a larger difference between children and adults because the pathway with the larger difference score would be expected to be further from the adult-like measurement.

We first performed a 5 (Pathway: VOF, VHP, PVP, DHP, FAT) x 2 (Age Group: children, adults) Repeated Measures ANOVA to determine if the nearness of children's FA to that of adults depended on the pathway. Second, we performed multidimensional scaling and *k*-means clustering using a distance matrix calculated from the PVP-VHP and PVP-DHP correlations. We tested the cohesiveness of tracts within the PVP, VHP, and DHP pathways by setting $k = 3$ and observing how tracts from each pathway clustered into three groups in children and adults. We tested the hypothesis that PVP microstructure was more similar to VHP microstructure than DHP microstructure in children by setting $k = 2$ and observing whether VHP or DHP tracts clustered with PVP tracts. Finally, we performed multiple linear regression analyses to determine if literacy and/or precursors of literacy (such as visual-motor and fine-motor skill; 93–99) predicted the microstructure of the PVP. **Table 1** reports descriptive statistics for behavioral measures for children and adults.

All ANOVAs and multiple linear regressions were performed using SPSS 25. All correlations and bootstrap tests were performed using Matlab R2019b. Matlab code that performs the post-processing analyses described in this study is available at https://github.com/svincibo/lwx-singleshell. Additional details for each analysis are provided in the **Results** section.

Definition of horizontal pathways, ventral and dorsal. We defined horizontal tracts as those tracts that connected anterior and posterior brain regions. The inferior fronto-occipital fasciculus (IFOF) is a horizontal tract that connects the prefrontal cortex and occipital cortex (64). The inferior longitudinal fasciculus (ILF) is a horizontal tract that connects the ventral temporal cortex with the occipital cortex (22, 63). The superior longitudinal fasciculus (SLF) is a large horizontal tract that connects the frontal motor and parietal cortex (132). The SLF can be segmented into two portions. SLF1and2 connect dorsal aspects of frontal cortex and superior parietal cortex; SLF3 connects ventral aspects of frontal

cortex and superior parietal cortex. Each of these horizontal tracts, IFOF, ILF, SLF1and2, and SLF3 connects an anterior portion of the brain to a posterior portion.

Horizontal tracts were further separated into ventral (IFOF, ILF) or dorsal (SLF1and2, SLF3) tracts because prior work has demonstrated that dorsal tracts undergo a more prolonged developmental trajectory than ventral tracts (33, 34, 36). While ventral tracts are adult-like by about 5 years of age, dorsal tracts may not be adult-like until about 20 years of age (33, 34, 36). We, therefore, expected to find a developmental difference between ventral and dorsal horizontal tracts, such that the ventral tracts were more adult-like in our child sample then dorsal horizontal tracts.

Definition of vertical pathways. We defined vertical tracts as those tracts that connected dorsal and ventral brain regions. The vertical occipital fasciculus (VOF) connects dorsal and ventral aspects of the occipital lobe (3, 17, 67, 133). The posterior arcuate (pArc) connects inferior parietal lobule with ventro-lateral portions of the middle portions of inferior and middle temporal gyri (16, 17, 64). The temporal parietal connection (TP-SPL) connects medial superior parietal lobule with ventro-lateral portions of the middle inferior temporal gyrus in the temporal cortex (18, 134). The middle longitudinal fasciculus (MdLF) is a large vertical tract that connects the parietal cortex and anterior temporal cortex (19). The MdLF can be segmented into two portions (21, 22). MdLFspl connects superior parietal lobule with anterior temporal cortex; MdLFang connects the inferior parietal lobule with anterior temporal cortex. The frontal aslant tract (FAT) is an anterior vertical tract that connects posterior superior frontal gyrus and posterior inferior frontal gyrus (64, 135).

We were primarily interested in vertical tracts that directly connect cortical regions traditionally associated with the ventral and dorsal visual streams--the tracts that comprise the PVP: pArc, TP-SPL, MDLFspl, MDLFang. The VOF and FAT were selected as comparison tracts for two reasons. First, we wanted to ensure that our findings were specific to tracts connecting ventral and dorsal visual streams rather than some quality of vertical tracts more generally. Second, the VOF is in the posterior brain while the FAT is in the anterior brain and, therefore, these two tracts bookend the proposed developmental progression from early visual regions (i.e., VOF) to later regions (i.e., FAT; **Figure 1**).

Results

Input-driven model of development in major white matter pathways

We propose an input-data driven model of white matter development by which the underlying mechanistic process of white matter development is driven by data input (**Figure 1b**). The model makes a step towards understanding the mechanisms that may underlie the development of white matter communication pathways. The insight behind the model can be most simply explained as “input-driven” because it proposes that data (i.e., input) is one of the primary driving forces behind white matter development. According to the model, we would expect white matter serving processing stages that mature early (i.e., occipital cortex) to mature earlier than white matter serving processing stages that mature late (i.e., temporal and parietal cortices; **Figure 1b;** 41–46). Hence, tracts communicating within the occipital lobe (1 in **Figure 1b**) and carrying information out of the occipital lobe (2 in **Figure**

1b) will mature earlier than tracts carrying information out of the ventral cortex (3 in **Figure 1b**). Using the same reasoning, tracts sending information out of the ventral cortex will mature earlier than tracts sending information out of the parietal cortex (4 in **Figure 1b**) and tracts within the frontal cortex (5 in **Figure 1b**). The proposed model of white matter development is consistent with the understanding of the role of white matter in learning and plasticity that has shown that training and increased use changes white matter microstructure (47–50).

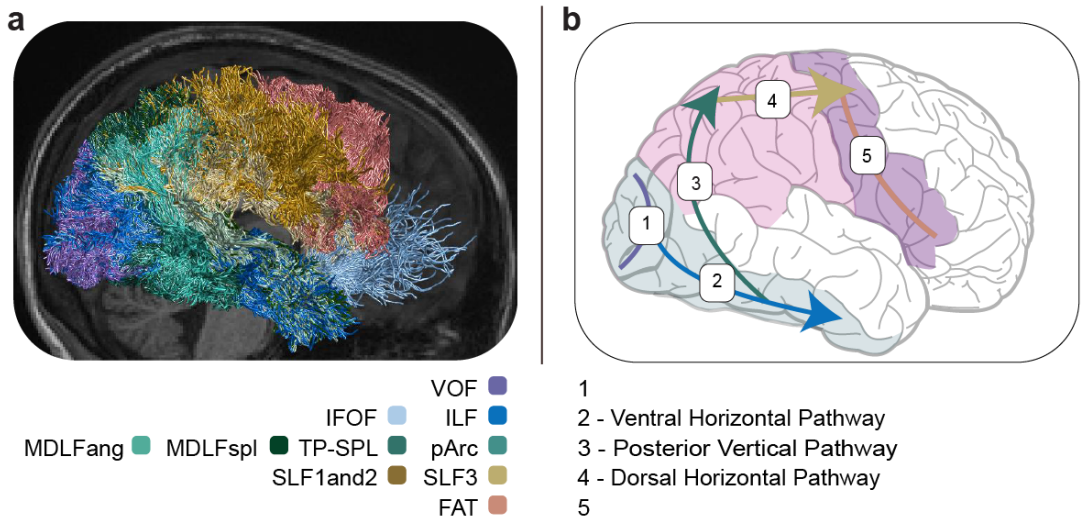

Figure 1. The input-driven model of white matter development. The input-driven model of white matter development posits that some portion of the development of white matter tracts is based on receiving input. **a. White matter tracts of interest displayed on an adult brain.** Tracts included in the ventral horizontal pathway (VHP; blues) included the ILF and IFOF. Tracts included in the posterior vertical pathway (PVP; greens) included the pArc, TP-SPL, MDLFspl, and MDLFang. Tracts included in the dorsal horizontal pathway (DHP; yellows) include SLF1and2 and SLF3. The VOF (purple) and FAT (salmon) were analyzed individually as representatives of the proposed earliest and latest developing tracts. They are also the only two tracts contained entirely within one lobe. **b. Developmental progression predicted by an input-driven model of white matter development.** The model predicts that white matter tracts earlier in the visual hierarchy would develop earlier than white matter later in the hierarchy (41–46; see **Results** for additional explanation). Anatomical tract tracing studies (51), developmental work on the horizontal white matter tracts (33, 36, 39, 40, 52, 53), and recent connectivity work (54), together, suggest that: Visual information first propagates through the occipital cortex (VOF) and (assuming no direct major white matter tract connecting the occipital to the parietal cortex; see **Results**), travels to the ventral temporal cortex. PVP tracts then carry the information to the parietal cortex and thereafter the dorsal horizontal tracts carry the information from the parietal cortex to the frontal cortex. The information likely carries onwards through the frontal cortex (FAT). According to the input-driven model of white matter development, the developmental progression of white matter tracts would be expected to proceed in this order: VOF, VHP, PVP, DHP, FAT.

Our model assumes that information from the occipital cortex travels to the ventral cortex and from there to the parietal cortex via the Posterior Vertical Pathway (PVP; **Figure 1b**). We note that the dorsal and ventral streams and their potential interactions are generally delineated based on functional and behavioral criteria (1, 2, 6, 8, 11, 55). Because of this, a major assumption in the literature has been that both the dorsal and ventral streams communicate *directly* from occipital to parietal and from occipital to ventral cortices, respectively (7, 54, 56, 57). There is, however, currently very little evidence for major white matter tracts between the occipital and parietal cortices in humans. The lack of evidence for major tracts between the occipital and parietal cortices is in stark contrast to an abundant literature on the major tracts between occipital and ventral cortices, such as the Inferior Longitudinal Fasciculus (ILF; 58–66). Although it is possible that a series of local U-fibers may convey information

between occipital and parietal cortices, as is the case in macaque (Felleman and Van Essen 1991; Baizer et al. 1991), these U-fibers have not been characterized and are likely to be plurisinaptic. In sum, there has been no report of a major white matter tract directly connecting occipital and parietal cortices in over 100 years of inquiry (3, 51, 54, 58, 67–69). One recent study specifically sought to find such a tract and was left wanting (54).

The input-driven model of white matter development proposed here (**Figure 1**) suggests that major white matter pathways develop in a particular order. The specific order that it proposes is that white matter tracts in occipital cortex (i.e., VOF) and in the ventral stream (i.e., Ventral Horizontal Pathway, VHP, including the ILF and IFOF) develop early, followed by tracts that connect the ventral stream to the dorsal stream (i.e., Posterior Vertical Pathway, PVP, including the pArc, TP-SPL, MDLFang, MDLFspl), and finally tracts in the dorsal stream (i.e., the Dorsal Horizontal Pathway, DHP, including the SLF1, SLF2, SLF3) and frontal cortex (FAT; **Figure 1a**). This developmental progression is consistent with two empirical findings. First, the microstructural tissue properties of white matter in the ventral-temporal cortex reach adult-like levels before white matter in parietal and frontal cortices while the microstructural properties of dorsal white matter undergoes a more prolonged developmental trajectory (33–36). Second, adult-like cortical function in posterior ventral-temporal cortices develops early compared to parietal and frontal cortices (70–72; but see also 73). Based on the known anatomical connections (see discussion in paragraph above), we would expect data to enter into the occipital cortex and then ventral-temporal cortex before proceeding onward to the parietal cortex and then frontal cortex, put explicitly: VOF, VHP, PVP, DHP, FAT (**Figure 1b**).

To provide evidence for the input-driven model of white matter development (**Figure 1**), we collected diffusion-weighted magnetic resonance imaging (dMRI) data in 24 children (5-8 years old) and 12 adults (18-22 years old) to obtain an estimate of fractional anisotropy (FA) for each pathway in children and in adults. We selected 5-8 years as the age range for our child sample because white matter microstructure and cortical function have been shown to be adult-like in the ventral-temporal cortex by 5 years of age (33–36). FA of the combined SLF1, 2 and 3, on the other hand, increases relatively slowly and plateaus at an adult-like measurement closer to 20 years of age (33–36). Given that white matter microstructure in the VOF and VHP would be expected to be adult-like in the 5-8 year old age range, the input-driven model of white matter development proposed here (**Figure 1**) would predict that the next pathway to become adult-like would be the PVP. The model would further predict that the PVP should be more adult-like than the DHP and FAT white matter tracts in children 5-8 years of age.

Reproducible data processing.

Anatomical and diffusion images were preprocessed using open and reproducible methods implemented as cloud services on brainlife.io (see **Table 2**; 74). Anatomical images were aligned to the AC-PC plane with an affine transformation and an age-appropriate atlas (75) and each participant's preprocessed diffusion image was then coregistered to their anatomical image (76). We fit the diffusion tensor model in a voxel-wise fashion to estimate fractional anisotropy (FA; 77) in each voxel before performing probabilistic tractography (78) to obtain a tractogram for each participant. The tractogram was segmented into 61 white matter tracts (79). We focused our analyses on the eight bilateral tracts comprising the PVP, DHP, and VHP, as well as bilateral VOF and FAT tracts, for a total of 20 tracts

(**Figure 2a**). We constructed a tract profile for each tract and for each participant that estimated FA along the tract (39, 80). The tract profiles for each tract were averaged across participants within each age group, resulting in a tract profile for each tract of interest for the child group and for the adult group (**Figure 2b**). All statistical analyses were performed using either pathway group means or tract group means. To obtain a tract group mean, we calculated the average FA along the group tract profiles, resulting in a mean FA value for each tract in each group. To obtain a pathway group mean, we calculated the average mean FA across tracts in each pathway, resulting in a mean FA value for each pathway in each age group (**Figure 2b**).

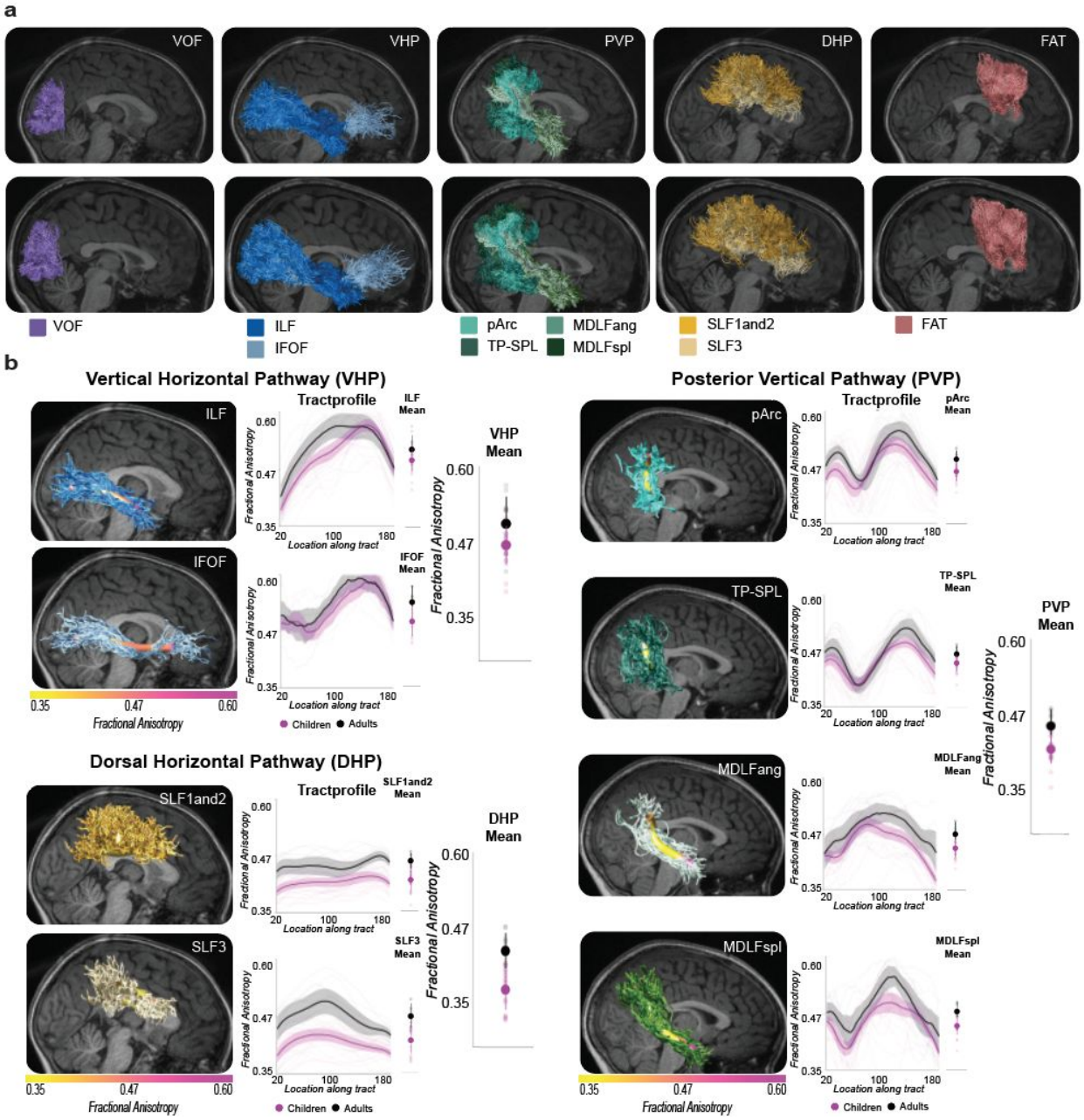

Figure 2. White matter pathway definitions and white matter microstructure feature extraction. a. Pathways and tracts of interest. Pathways are displayed on representative child (top) and adult (bottom) brains. Both left and right

hemispheres were evaluated; however, only the right hemisphere is displayed in the figure. Tracts were visualized using https://github.com/francopestilli/mba (81). **b. Tract profiles analysis.** A tract 'core' was estimated for each tract in individual brains using the tractprofiles approach (39) implemented on brainlife.io (80). FA at each node of the core was estimated by averaging across streamlines at that node and weighting by the distance of the streamline from the 'core'. In the tract profile plots, FA is displayed on the y-axis; location along the tract 'core' is displayed on the x-axis. To calculate the mean FA for a tract, we averaged across the core FA values, excluding the first and last 20 nodes to avoid partial voluming effects. To calculate the mean FA for a pathway, we averaged the mean tract FA values for tracts included in that pathway. For example, in the ventral horizontal (VHP) pathway, the mean FA for the ILF and IFOF were averaged to obtain the mean FA for the VHP pathway. We provide depictions of these analyses for each of the three pathways: the VHP pathway (top left), the dorsal horizontal (DHP) pathway (bottom left), and the posterior vertical pathway (PVP) (right).

Analysis 1. Vertical posterior tracts become adult-like before dorsal horizontal tracts

Our input-driven model of white matter development would predict that the development of white matter pathways should depend on the location of the pathway in the processing hierarchy, with pathways closer to sensory input (e.g., VOF or VHP) reaching adult-like microstructural values earlier than pathways further from sensory input (e.g, FAT or DHP; **Figure 1b**). More specifically, it predicts that in children 5-8 years of age, the PVP should be more adult-like than the DHP and the FAT. We expected that the VOF and VHP would be adult-like in children of this age range based on prior literature (33–36). We performed a Two-Way Repeated Measures ANOVA to determine if there were any age group differences in white matter microstructure that depended on the pathway (**Figure 2a**). The age-group difference was an estimate of how adult-like a particular pathway was in our sample. The smaller the difference, the more adult-like the microstructure of the pathway; the larger the difference, the less adult-like the microstructure of the pathway. The dependent variable was the mean FA along a tract's profile, averaged across all tracts within that pathway and across hemispheres (**Figure 2**). The first factor, PATH, had five levels that were entered in this order: VOF, VHP, PVP, DHP, FAT. The second factor, AGE, had two levels: children and adults. PATH was within-participants and AGE was between- participants. SEX was entered as a covariate of no interest (52, 53).

We predicted an interaction between AGE and PATH–that the magnitude of the difference in FA between children and adults would depend on the factor PATH. More specifically, we predicted a linear trend in the difference in FA between children and adults such that the size of the difference in FA between children and adults would follow the order proposed by the model (**Figure 1b**), namely, VOF, VHP, PVP, DHP, and FAT.

Results were in line with our predictions (**Figure 3**), suggesting that the maturation of the pathways proceeds from early to late pathways as would be predicted by our input-driven model of white matter development (**Figure 1**). The Two-Way Repeated Measures ANOVA revealed an interaction between PATH and AGE, $F(4, 132) = 4.109$, $p = 0.004$. The main effect of PATH was significant, $F(4, 132) = 19.473$, $p = 0.000$. The main effect of AGE was significant, $F(1, 33) = 26.928$, $p = 0.000$. The significant interaction was driven by a linear trend, $F(4, 33) = 9.723$, $p = 0.004$; no other trends were significant. Post-hoc independent samples t-tests demonstrated that the significant linear trend was an increase in the difference in FA between children and adults across PATH, in the predicted order: VOF, $t(34) = 3.013$, $p = 0.005$, VHP, $t(34) = 2.725$, $p = 0.010$, PVP, $t(34) = 4.297$, $p = 0.000$, DHP, $t(34) = 5.685$, $p = 0.000$, and FAT, $t(34) = 4.680$, $p = 0.000$. All post-hoc independent samples t-tests passed Bonferroni

correction for 5 comparisons at the $p = 0.01$ significance level (i.e., 0.05/5 = 0.01), except the *t*-tests for VOF and VHP tracts. PATH did not interact with SEX, $F(4, 132) = 1.041$, $p = 0.389$, our covariate of no interest. A Levene's Test suggested that the error variance was not unequal across age groups, all *p*s > 0.05, indicating that a standard ANOVA and *t*-test were appropriate for these data.

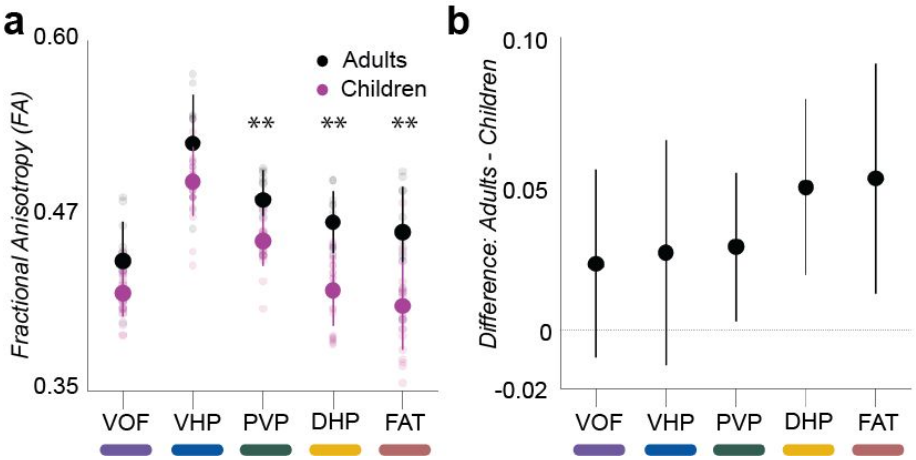

Figure 3. Interaction between Pathway and Age Group. a. Group means for each pathway. Group means for each pathway overlaid on individual participant means (transparent dots) color coded for age group. Adult means are shown in black and child means are shown in pink. The difference in fractional anisotropy (FA) between children and adults was dependent on Pathway. The age difference in FA increased linearly from the vertical-occipital fasciculus (VOF), to ventral horizontal tracts in the ventral visual stream (VHP), to the vertical posterior tracts that connect the ventral stream to parietal cortex (PVP), to dorsal horizontal tracts that connect parietal cortex to frontal motor cortex (DHP), and to the frontal aslant tract (FAT) that connects dorsal and ventral frontal motor cortex. **b. Difference in group means for each pathway.** Difference in group means are displayed for reference. Error bars represent standard deviation. **, $p < 0.05$ Bonferronni corrected.

In sum, this result indicates that PVP microstructure was more adult-like than the DHP and FAT, consistent with the input-driven model of white matter development (**Figure 1a**) and demonstrates that PVP microstructure was not yet adult-like in our child sample. In addition, the results are consistent with previous reports (33, 34) in that they revealed that the microstructure of tracts in the VHP was adult-like and was more adult-like than the microstructure of tracts in the DHP. In our child sample, the VHP is adult-like, the PVP is less adult-like, and the DHP is even less adult-like.

Three additional analyses were also performed to further investigate whether these results depended on hemisphere (**Analysis 1.1**), tract within pathway (**Analysis 1.2**), and age within the child group (**Analysis 1.3**). We found no evidence of hemispheric asymmetry. We found no evidence of tract-related heterogeneity within any pathway. We found no evidence of age-related heterogeneity in our child sample, validating the combination of all children into one age group.

Analysis 1.1 Hemispheric differences

We found no evidence of hemispheric asymmetry. A 5 (PATH: VOF, VHP, PVP, DHP, FAT) x 2 (Age Group: Children, Adults) x 2 (Hemisphere: Left, Right) Repeated Measures ANOVA with Sex entered as a covariate of no interest revealed a significant main effect for PATH, $F(4, 132) = 20.074$, $p = 0.000$, and a significant two-way interaction between PATH and Age Group, $F(4, 132) = 4.063$, $p = 0.004$, as in

the original Two-Way Repeated Measures ANOVA. The three-way interaction, however, was not significant, $F(4, 132) = 0.396$, $p = 0.811$, post hoc observed power = 0.139, suggesting that the difference between children and adults among tract categories did not depend on hemisphere. Post hoc 5 (PATH: VOF, VHP, PVP, DHP, FAT) x 2 (Age Group: Children, Adults) Repeated Measures ANOVAs with Sex entered as a covariate of no interest were conducted for each hemisphere separately. These post hoc ANOVAs revealed a significant linear interaction in both the left, $F(1, 33) = 6.380$, $p = 0.017$, and the right hemispheres, $F(1, 33) = 9.116$, $p = 0.005$; both linear interactions were in the same direction, with the difference in FA between children and adults across PATH increasing in the predicted order: VOF, VHP, PVP, DHP, FAT.

Analysis 1.2 Pathway cohesion

We found no evidence of tract-related heterogeneity within any pathway. We performed a Two-Way Repeated Measures ANOVA for each PATH that included two factors, Tract and Age Group. Tract had as many levels as tracts that were included in that PATH. Age Group always had 2 levels, children and adults. The dependent variable was always fractional anisotropy (FA). Results for each pathway are reported separately. *Ventral Horizontal (VHP) Tracts.* A Two-Way Repeated Measures ANOVA for Tract (L-ILF, L-IFOF, R-ILF, R-IFOF) and Age Group (children, adults) with Sex entered as a covariate of no interest revealed a significant main effect of Age Group, $F(1, 10) = 21.709$, $p = 0.001$. The main effect of Tract was not significant, $F(3, 30) = 0.743$, $p = 0.535$. The interaction between Tract and Age Group was not significant, $F(3, 30) = 1.207$, $p = 0.324$, post hoc power for alpha = 0.05 at 0.290, suggesting that the difference between children and adults did not differ among tracts that were included in the VHP. *Vertical Posterior (PVP) Tracts.* A Two-Way Repeated Measures ANOVA for Tract (L-pArc, L-TP-SPL, L-MDLFspl, L-MDLFang, R-pArc, R-TP-SPL, R-MDLFspl, R-MDLFang) and Age Group (children, adults) with Sex entered as a covariate of no interest revealed a significant main effect of Tract, $F(7, 224) = 3.913$, $p = 0.000$, and of Age Group, $F(1, 32) = 18.194$, $p = 0.000$. The interaction between Tract and Age Group was not significant, $F(7, 224) =1.622$, $p = 0.130$, post hoc power for alpha = 0.05 at 0.665, suggesting that the difference between children and adults did not differ among tracts that were included in the PVP. *Dorsal Horizontal (DHP) Tracts.* A Two-Way Repeated Measures ANOVA for Tract (L-SLF1and2, L-SLF3, R-SLF1and2, R-SLF3) and Age Group (children, adults) with Sex entered as a covariate of no interest revealed a significant main effect of Age Group, $F(1, 33) = 30.584$, $p = 0.000$. The main effect of Tract was not significant, $F(3, 99) = 1.885$, $p = 0.137$. The interaction between Tract and Age Group was not significant, $F(3, 99) = 1.500$, $p = 0.219$, post hoc power for alpha = 0.05 at 0.386, suggesting that the difference between children and adults did not differ among tracts that were included in the DHP pathway.

Analysis 1.3 Age group cohesion

We found no evidence of age-related heterogeneity in our child sample, validating the combination of all children into one age group: children. A 5 (PATH: VOF, VHP, PVP, DHP, FAT) x 2 (Age Group: Children 4.5 - 6.5 years, Children 6.5 - 8.5 years) Repeated-Measures ANOVA with Sex entered as a covariate of no interest revealed a significant main effect of PATH, $F(4, 84) = 13.250$, $p = 0.000$; however, neither the main effect of Age Group nor the interaction between PATH and Age Group were significant, $F(1, 21) = 2.878$, $p = 0.105$, post hoc power for alpha = 0.05 at 0.367, and $F(1, 21) = 0.399$,

p = 0.809, post hoc power for alpha = 0.05 at 0.138, respectively. The covariate SEX was also not a significant predictor of FA, $F(1, 21) = .363$, $p = 0.553$, and SEX did not interact with PATH, $F(1, 21) = .011$, $p = 0.918$. The lack of a statistically significant difference between the two age-groups (Age Group: Children 4.5 - 6.5 years, Children 6.5 - 8.5 years) in the first ANOVA, justified the inclusion of all children into one age group as in **Analysis 1**, as well as the following analyses (**Analyses 2** and **3)**.

However, we were surprised to find no age-group differences in the child sample and performed additional tests to assess age-related differences within the children, collapsing across age groups. We performed a linear regression to assess age-related heterogeneity using age as a continuous predictor. The dependent variable was fractional anisotropy (FA). Predictors included AGE as a continuous variable, PATH as a categorical variable, and the interaction between AGE and PATH. Sex was included as a dichotomous covariate of no interest. FA was significantly predicted by the model, $F(4, 106) = 2.910$, $p = 0.025$, with $R^2 = 0.102$ and $R_{adjusted} = 0.067$. The full model and resulting parameters were: Predicted FA = 1.941 - 0.27(AGE) - 2.94(PATH) + 0.004(AGE*PATH) + 0.158 (SEX). Each predictor was tested for significance using a one-sample *t*-test and a threshold of $p < 0.05$, using a Bonferroni correction for the 3 comparisons (i.e., the 3 predictors), $p_{Bonferroni} = 0.05/3 = 0.017$. There were no significant predictors after Bonferroni correction for multiple comparisons, all *p*s > 0.017. To further investigate the apparent absence of an effect of AGE in the child group, we conducted the linear regression with the interaction term removed: Predicted FA = 1.012 - 0.016(AGE) - 0.003(PATH) + 0.163 (SEX). The overall model was significant, $F(3, 106) = 3.521$, $p = 0.018$. AGE was significant, $p = 0.004$, but PATH was not, $p = 0.961$, and SEX was not, $p = 0.319$.

Analysis 2. PVP tracts cluster with VHP tracts in children but not in adults

According to the input-driven model (**Figure 1**), during development the microstructure of a particular tract should be more associated with the tracts in the pathway from which it receives feed-forward inputs than tracts in pathways to which it sends inputs. The PVP is the first pathway in the processing hierarchy to demonstrate a difference between children and adults; it is preceded by an adult-like VHP and followed by a non-adult-like DHP (**Figure 3; Analysis 1**). Here, we investigate the hypothesis that PVP microstructure is related to the maturation of the data that it carries. More specifically, tracts carrying information out of the ventral cortex (PVP; 3 in **Figure 1b**) will be more similar to the mature tracts carrying information to the ventral cortex (VHP; 2 in **Figure 1b**) than the relatively immature tracts carrying information out of the parietal cortex (DHP; 4 in **Figure 1b**). To this end, we employed multi-dimensional scaling (MDS) followed by *k*-means clustering to assess whether PVP microstructure would be more similar to the VHP that precedes it or the DHP that follows it.

To prepare the data for *k*-means clustering, pairwise Pearson's correlations (*r*) between tracts were computed based on z-scored FA values (**Figure 4**). The FA values were z-scored by computing the mean and standard deviation within each tract and group. We then grouped the pairwise correlations into one of two categories: (1) correlations between PVP and VHP tracts (**Figure 4;** blue frame) and (2) correlations between PVP and DHP tracts (**Figure 4;** yellow frame). We transformed the pairwise correlations into distance values (*d*) by computing the Euclidean distance between PVP-VHP and PVP-DHP correlation pairs and used *d* to perform classical multidimensional scaling (MDS; 84–88).

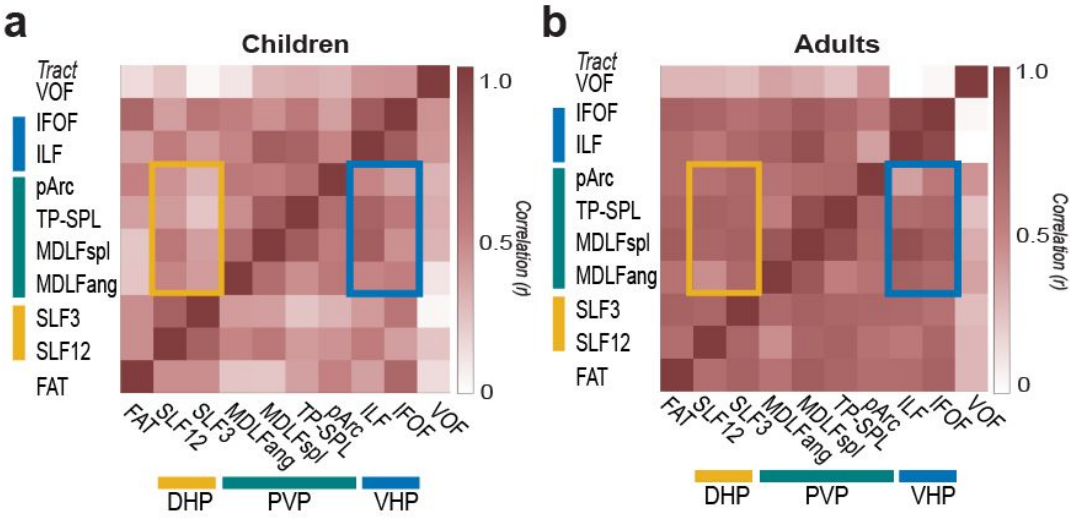

Figure 4. Pairwise correlation matrices of white matter tract microstructure. a. Pairwise correlations in children. b. Pairwise correlations in adults. Pairwise correlations are between microstructure properties (FA) between tracts assigned to dorsal horizontal, ventral horizontal, and posterior vertical pathways. Tracts in the posterior vertical pathway (PVP) are indicated with a green bar. Tracts in the dorsal horizontal pathway (DHP) are indicated with a yellow bar and tracts in the ventral horizontal pathway (VHP) are indicated with a blue bar. In this analysis, a positive correlation between two tracts suggests that children with higher FA in one tract would also have higher FA in the second tract.. Correlations among PVP and VHP tracts are framed in blue while correlations among PVP and DHP tracts are framed in yellow. All correlations were positive.

MDS was used to decompose the distance values into independent dimensions that could be used for *k*-means clustering (84, 89). A scree plot of the eigenvalues for each dimension in the MDS results and the final maximum relative error (*MRE*) of the model were used to select the appropriate number of dimensions (90). The scree plot showed that both child and adult models were well specified by the first dimension (i.e., high eigenvalue in the first dimension relative to the other dimensions; **Figure 5a**). Including the second dimension, however, reduced the *MRE* by approximately half in both child and adult samples (first dimension alone: 0.67 in children and 0.55 in adults, first and second dimensions: 0.34 and 0.32; **Figure 5a**). Together, the scree plot and *MRE* values suggested that models using the first two dimensions were substantially better specified than those using only the first dimension in both data sets. Because of this, the first two dimensions were used for *k*-means clustering.

To assess how well the tracts clustered into our three defined pathways (VHP, PVP, DHP; see **Analysis 1.2** for a similar test), *k*-means clustering ($k = 3$) was applied to the first two dimensions of the MDS model. *k*-means was performed 10,000 times and the clustering result with the lowest Sum of Squared Distances (*SSD*) of the data points from the centroids was selected as the winning model (84, 89). A silhouette score was calculated to estimate how closely the data points clustered around the centroids within each cluster in the winning model (91). Results in children demonstrated that the VHP, PVP, and DHP tracts clustered into separated clusters (**Figure 5b top**). The model *SSD* was 0.366. The silhouette scores of the VHP cluster, the PVP cluster, and the DHP cluster were 0.709, 0.625, and 0.816, respectively, indicating that the clustering solution was appropriate.

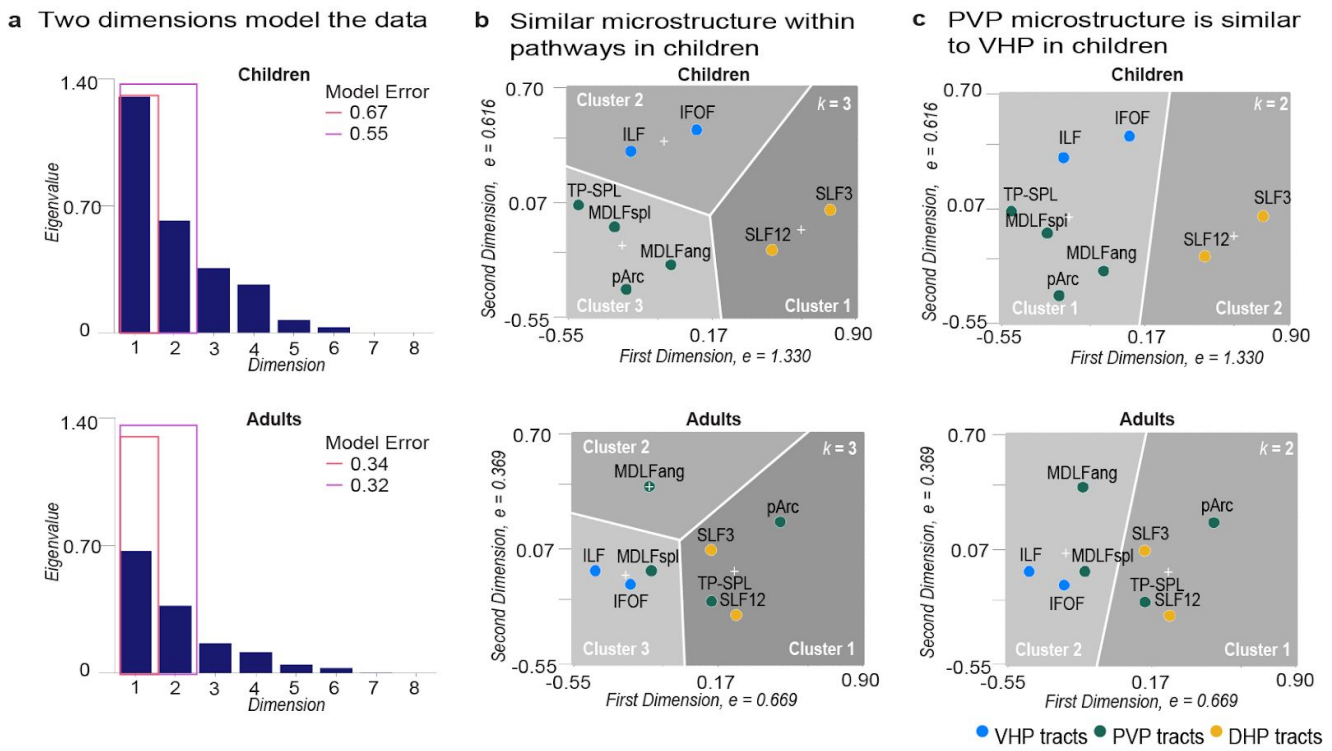

Figure 5. Multidimensional scaling of PVP-VHP and PVP-DHP correlations. a. PVP correlations were modelled well using the first two MDS dimensions. MDS eigenvalues were positive and large and suggested that the MDS models were able to explain a large portion of the variance in both child and adult data using only the first dimension. Eigenvalues were larger for the child data than for the adult data, suggesting that MDS was able to detect dimensionality better in the child data than in the adult data. The max relative error (*MRE*) values suggested that including the second dimension substantially increased the model fit. **b. Separate clusters for VHP, PVP, and DHP tracts in children but not adults.** *k*-means clustering with *k* = 3 was performed to test tract membership in the ventral horizontal (VHP), posterior vertical (PVP), and dorsal horizontal (DHP) pathways. The analysis affirmed that the VHP, PVP, and DHP tracts clustered into their own clusters in the child data, but this was not the case for the adult data. **c. Common clusters for VHP and PVP tracts in children but not adults.** *k*-means clustering with *k* = 2 was performed to test the hypothesis that PVP microstructure would be more similar to VHP than DHP microstructure. The results demonstrated that PVP and VHP tracts clustered together while the DHP tracts remained in their own cluster in children, but this was not the case for adults. Cluster centroids are displayed as white crosses.

Results in adults demonstrated that the MDLFspl tract clustered with the VHP tracts, that the pArc and TP-SPL clustered with the DHP tracts, and that the MDLFang was in a cluster of its own (**Figure 5b bottom**). The model *SSD* in adults was 0.293. The silhouette scores of clusters 1, 2, and 3 were 0.827, 0.469, and 1, respectively. The similarity between tracts from the same pathway was greater than the similarity between tracts from different pathways in the child sample (**Figure 5b**), suggesting that the VHP, PVP, and DHP can be treated as distinct pathways in our child sample (consistent with **Analysis 1.2**).

To assess our prediction that PVP microstructure would be more similar to the microstructure of the upstream VHP relative to microstructure in the DHP in children, a *k*-means clustering (*k* = 2) algorithm was applied to the first two dimensions of the MDS model. Results were as predicted. In children, PVP and VHP tracts clustered together while the DHP tracts clustered separately (**Figure 5c top**),

suggesting that the microstructure of PVP tracts were more similar to the microstructure of VHP tracts than DHP tracts in children. The model *SSD* was 0.866. The PVP-VHP cluster had a silhouette score of 0.575 and the DHP cluster had a silhouette score of 0.834. In adults, two PVP tracts clustered together with the VHP tracts, the MDLFspl and the MDLFang, and two PVP tracts clustered together with the DHP tracts, the pArc and the TP-SPL (**Figure 5c**). The model *SSD* was 0.479. Cluster 1 had a silhouette score of 0.606 and cluster 2 had a silhouette score of 0.559. Thus, the PVP and VHP clustered together in children but not in adults, suggesting that the microstructure of the PVP is more similar to the microstructure of the VHP than the DHP in children.

Analysis 2.1 Hemispheric cohesion

MDS models for the left and right hemispheres independently were also tested. We compared the *SSD* values of the MDS fits to determine if hemisphere-specific models would be better suited for the data than models that included both hemispheres. We performed this comparison using the first two dimensions of the MDS results. The hemisphere specific models had either higher *SSD* values than both hemispheres in children (left: 0.43, right: 0.53, both: 0.35) or *SSD* values similar to both hemispheres in adults (left: 0.30, right: 0.27, both: 0.32), suggesting that MDS performed on both hemispheres produced a better or similar model fit than MDS performed on each hemisphere separately. For these reasons, the main analyses (**Analysis 2**) were performed using both hemispheres together.

Analysis 2.2 Bootstrap test of difference between PVP-VHP and PVP-DHP correlations

We performed an additional analysis to assess whether the correlation among PVP and VHP tracts was greater than the correlation among PVP and DHP tracts using a bootstrap test of the difference between the mean PVP-VHP and PVP-DHP correlations (see **Figure 4**). Results showed that the PVP-VHP correlations were greater than the PVP-DHP correlations in children, $z = 2.145$, $p = 0.016$, but not in adults, $z = 0.073$, $p = 0.471$, consistent with the MDS and *k*-means results (**Figure 5c**).

Analysis 3. Performance on a visual perceptual task predicts PVP microstructure in children

Results from Analyses 1 and 2 suggest that the age range of the child sample is likely a period of significant developmental change for the PVP. The PVP was the first white matter pathway in the proposed developmental progression (**Figure 1b**) that was not adult-like (**Figure 3**). The PVP microstructural properties were also more strongly associated with the microstructure of the VHP that precedes it than the DHP that follows it in the child sample (**Figure 5c**). These results and the input-driven model (**Figure 1**) suggest that PVP microstructural development might be driven by experience. Therefore, we investigated whether individual differences in PVP microstructure were related to behavioral measures of learning in the child sample.

The few studies that have looked at the development of white matter in the PVP have focused on the relationship between the pArc microstructure and literacy. An association between reading and FA in the pArc is often reported in children 7 years and older (26–32). Research concerning PVP behavioral correlates in children younger than 7 years, however, is extremely limited but suggests a similar

association. One cross-sectional study in 5-8 year old children found that the microstructure of the pArc correlated positively with literacy (83). Another study using children of the same age range found that one year of literacy instruction resulted in microstructural changes in voxels that likely overlap with the PVP. In addition, the size of the microstructural change correlated positively with children's literacy gains over the one-year period (92). While the evidence for a relationship between literacy and microstructure of tracts in the PVP in children younger than 7 years is still emerging, current work suggests that the information conveyed along the PVP is likely related to the early stages of learning to read.

We first assessed the relationship between the average FA values across all tracts within the PVP and behavior. To explore potential relationships between PVP microstructure and early literacy skills, a multiple linear regression analysis was performed to predict PVP microstructure in our child sample using three composite scores generated from different behavioral assessments that measured: literacy, visual-motor skill, and fine-motor skill (see **Materials and Methods** for a description of how the composite measures were computed). A large amount of work suggests an association between microstructure of PVP tracts and reading in children 7 years and older (26–32); however, our sample was 5-8 years of age. We, therefore, included visual-motor and fine-motor skill measures in the regression because a large amount of work has demonstrated that these two skills positively predict future literacy attainment (93–99). The dependent variable was the z-scored microstructural property (i.e., FA), averaged across tracts within the PVP, and the independent variables were the z-scored behavioral composite measures, as well as age in months and sex, excluding interaction terms. Only linear terms were included, because linear fits are most appropriate for this age range (100). The regression model was tested for significance using an *F*-test of the overall model fit with the significance threshold set to $p < 0.05$. Each predictor was tested for significance using a one-sample *t*-test and a threshold of $p < 0.05$, using a Bonferroni correction for the 3 comparisons (i.e., the 3 predictors), $p_{Bonferroni} = 0.05/3 = 0.017$. Results demonstrated that PVP microstructure was related to visual-motor and fine-motor skill in the child sample. FA in the PVP was significantly predicted by the model, $F(5, 22) = 3.117$, $p = 0.035$, with $R^2 = 0.478$ and $R_{adjusted} = 0.325$. The full model and resulting parameters were: Predicted FA = 1.744 + 0.579(VM) - 0.420(FM) + 0.441(LIT) - 0.012(AGE) - 0.590(SEX). There were no significant predictors after Bonferroni correction for multiple comparisons, all *p*s > 0.017. AGE and SEX were also not significant predictors, all *p*s > 0.05.

After testing a model using the average FA across PVP tracts, we clarified the relationship between individual PVP tracts and behavior. To determine if a particular tract within the PVP was driving the relationship between FA in PVP and the behavioral measures, four multiple linear regressions were performed for each PVP tract separately. Models were specified as described in the previous section and a Bonferroni correction was used to assess significance. Only one of the four models was significant. Results revealed a significant relationship between behavior and the pArc (**Figure 6a**), $F(5, 22) = 4.435$, $p = 0.009$, with $R^2 = 0.752$ and $R_{adjusted} = 0.438$. The full model and resulting parameters were: Predicted FA = -0.217 + 0.782(VM) - 0.718(FM) + 0.109(LIT) - 0.011(AGE) + 0.794(SEX). Both VM and FM were significant predictors of FA in the pArc, VM: $t(22) = 3.137$, $p = 0.006$ and FM: $t(22) = -2.822$, $p = 0.012$. SEX, a covariate of no interest, was also a significant predictor of FA in the pArc, $p = 0.016$. We note that these results pass a multiple correction threshold correcting for the number of

variables tested (3, p = 0.017), but not when correcting for number of variables and models (4) tested altogether (12 total, p = 0.004). To conclude this model found a significant relationship between FA in the pArc and the visual-motor skill and fine-motor skill composite scores (**Figure 6a**).

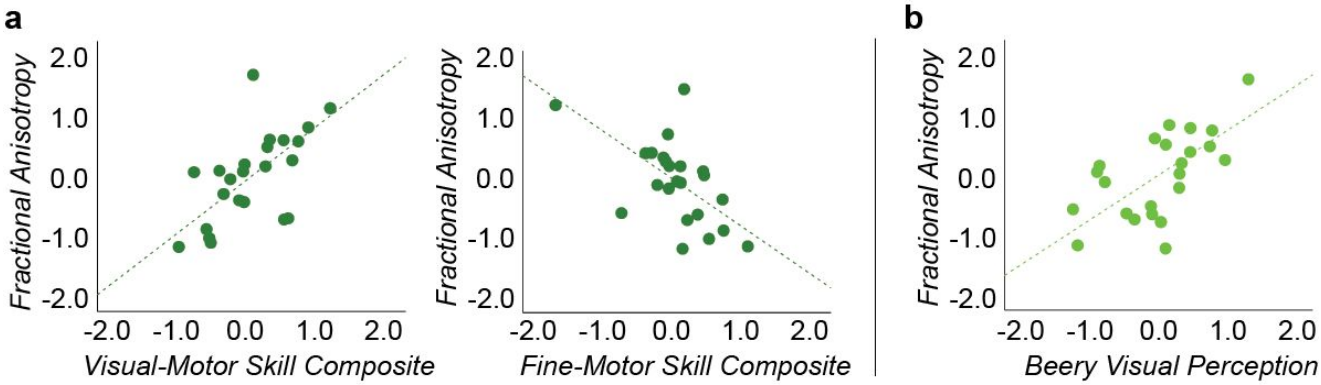

Figure 6. Performance on a visual perceptual task predicts FA in the posterior arcuate (pArc) in the child sample. a. Relationship between pArc FA and Visual-motor and Fine-motor Skill. Fractional anisotropy (FA) in the pArc was positively predicted by the VM composite score and negatively predicted by the FM composite score. **b. Relationship between pArc FA and performance on Beery Visual Perception.** Performance on the Beery Visual Perception (Beery VP) subtest positively predicted FA in the pArc. The Beery VP is one of three subtests used to calculate the VM composite score referenced in **a**. All measurements were based on the child sample and were z-scored.

We further investigated these composite scores because we found that the visual-motor (VM) and fine-motor (FM) skill scores were significant predictors of FA in the pArc. A single, follow-up multiple linear regression was specified to predict FA in the pArc from all subtests that comprised the VM and FM composite scores (see **Materials and Methods: Behavioral Assessment**). The VM composite score consisted of Visual Perception (VP), Motor Coordination (MC), and Visual-Motor Integration (VMI) subtests. The FM composite score consisted of Grooved Pegs-R and Grooved Pegs-L subtests. The LIT composite score was not tested further because it was not identified as a significant predictor of FA in the pArc (see previous analysis). Age and sex were entered as covariates of no interest. A multiple comparison Bonferroni correction was applied (5 comparisons, one per predictor of interest, $p_{Bonferroni}$ = 0.05/5 = 0.010). The model fit was significant, $F(7, 22) = 3.410$, $p = 0.022$, with $R^2 = 0.784$ and $R_{adjusted}$ = 0.614. The full model and resulting parameters were: Predicted FA = -1.1276 + 0.078(Beery VMI) + 0.644(Beery VP) + 0.135(Beery MC) + 0.577(GroovedPegs-R) - 0.259(GroovedPegs-L) + 0.005(AGE) + 0.104(SEX). Results revealed that performance on the Beery VP assessment significantly predicted FA in the pArc (**Figure 6b**; $t(22) = 3.031$, $p = 0.008$). GroovedPegs-R was marginally significant, but did not pass multiple comparisons corrections, $t(22) = 2.171$, $p = 0.046$. There were no other significant predictors, all ps > 0.010. We conclude that FA in the pArc of our child sample can be predicted by Beery Visual Perception scores; as FA increases, performance on Beery Visual Perception increases.

Testing for hemispheric asymmetry and non-PVP pathways

We performed two additional analyses to better understand if our results could be explained by one hemisphere alone (**Analysis 3.1**) to see if a relationship with behavior could be found in pathways other than the PVP (**Analysis 3.2**).

Analysis 3.1 Hemispheric cohesion

We further tested for evidence of hemispheric asymmetry in the relationship between microstructure in the pArc and behavior. The left pArc was significantly predicted by behavior, but we did not find a significant relationship between the right pArc and behavior. For each hemisphere, we tested a linear model that predicted FA from the composite measures of LIT, VM, and FM that were used in the previous analyses. SEX was entered as a covariate of no interest. *Left Hemisphere.* The model fit for the left pArc was significant, $F(5, 22) = 4.898$, $p = 0.006$, with $R^2 = 0.590$ and $R_{adjusted} = 0.470$. There were no significant predictors after Bonferroni correction, all *p*s > 0.017; however, the VM and FM composite scores trended towards significance with VM positively predicting FA in the pArc, $t(22) = 3.135$, $p = 0.006$, and FM negatively predicting FA in the pArc, $t(22) = 3.571$, $p = 0.002$. *Right Hemisphere.* The model fit for the right pArc was significant, $F(5, 22) = 1.867$, $p = 0.153$, with $R^2 = 0.595$ and $R_{adjusted} = 0.165$, but there were no significant predictors, all *p*s > 0.017.

Analysis 3.2 Behavioral correlates of non-PVP pathways

We performed the same multiple linear regression analysis described for the PVP for the other four pathways of interest: VOF, VHP, DHP, and FAT. None of the model fits were significant and there were no significant predictors. *Vertical Occipital Fasciculus (VOF).* The model fit was not significant, $F(5, 22) = 0.624$, $p = 0.684$, with $R^2 = 0.155$ and $R_{adjusted} = -0.094$, and there were no significant predictors, all *p*s > 0.017. *Ventral Horizontal Tracts (VHP).* The model fit was not significant, $F(5, 22) = 1.070$, $p = 0.411$, with $R^2 = 0.239$ and $R_{adjusted} = 0.016$, and there were no significant predictors, all *p*s > 0.017. *Dorsal Horizontal Tracts (DHP).* The model fit was not significant, $F(5, 22) = 1.050$, $p = 0.421$, with $R^2 = 0.236$ and $R_{adjusted} = 0.011$, and there were no significant predictors, all *p*s > 0.017. *Frontal Aslant Tract (FAT).* The model fit was not significant, $F(5, 22) = 1.670$, $p = 0.196$, with $R^2 = 0.329$ and $R_{adjusted} = 0.132$, and there were no significant predictors, all *p*s > 0.017.

Discussion

The degree of functional interaction between the ventral and dorsal streams has been discussed in multiple scientific domains for decades (1, 2, 6, 8–11). Communication between the two streams may be mediated by the white matter tracts connecting the cortical areas in each stream and may be important for cortical development in both streams. Understanding the role of white matter connections within and between the streams can help us understand their degree of interaction and how this might change over the course of the development.

We investigated the microstructure of the white matter tracts within and between the two streams in children and adults. In the domain of white matter tracts and connectivity, horizontal tracts *within* each stream (dorsal or ventral) have been studied extensively (see reviews on gestation (101, 102), infancy (102, 103), childhood and adolescence (100, 104), adulthood (105, 106), and geriatrics (107)). Opposite to that, relatively little attention has been paid to the vertical tracts that run *between* the dorsal and ventral streams (**Figure 1a**; 25). Consequently, we know very little about vertical tracts and even less about their development. We focused on a specific vertical pathway in the posterior brain, the PVP. The PVP is comprised of 4 white matter tracts that directly connect tracts in the ventral horizontal pathway (VHP; i.e., ILF, IFOF) with tracts in the dorsal horizontal pathway (DHP; i.e., SLF1and2,

SLF3).

Our results, collectively, support an input-driven model of white matter development (**Figure 1**) and suggest that the PVP might facilitate interactions between dorsal and ventral visual streams during development (14, 15). We first demonstrated that the difference between child and adult microstructure increased linearly from early to late pathways: VOF, VHP, PVP, DHP, FAT (**Figure 3**). The PVP was the earliest pathway to demonstrate a difference in microstructure between children and adults (**Figure 3a**), suggesting that the PVP was actively undergoing developmental change in our child sample. In addition, this first analysis demonstrated that VHP microstructure was already adult-like in our child sample, consistent with prior work (**Figure 3**; 33, 34, 36). We then demonstrated that PVP microstructure was more similar to VHP than to DHP microstructure in our child sample (**Figure 5c**). The results of this second analysis (**Figure 5**), given the developmental context established by the first analysis (**Figure 3**), suggest that white matter pathways may develop in response to incoming communication from relatively mature upstream pathways. Finally, we demonstrated that FA in the pArc, a PVP tract connecting posterior ventral-temporal and inferior parietal cortices was uniquely predicted by performance on a perceptual matching task, suggesting that the PVP may facilitate interactions between ventral and dorsal visual streams during learning.

We show that white matter tracts cluster together into cohesive multi-tract pathways and development in the age range of our child sample (i.e., 5-8 years) happens at the pathway-level. The results of the MDS and *k*-means clustering analysis validated our pathways approach for the VHP, PVP, and DHP that was used in our primary analyses. We expected the ILF, IFOF, pArc, TP-SPL, MDLFspl, MDLFang, SLF1and2, and SLF3 to cluster into the VHP, PVP, and DHP pathways and we, therefore, set $k = 3$. Results support the pathway approach in our child sample (**Figure 5b**) but not necessarily in adults. Finding that tracts cluster into the predicted pathways in the child sample but not in the adult sample suggests that the relationship among tracts within a pathway is more homogeneous in childhood than adulthood (see **Analysis 1.2** for a similar finding).

The PVP was the first pathway in our proposed trajectory (**Figure 1b**) pathway to demonstrate a significant microstructural difference between children and adults (**Figure 3a**), suggesting that the PVP undergoes active development in the 5-8 year old age range, and perhaps throughout adolescence. We focused on the PVP and the pathways immediately upstream (VHP) and downstream (DHP) of the PVP to better understand the developmental relationship among VHP, PVP, and DHP white matter. Based on the input-driven model of white matter development (**Figure 1a**), we hypothesized that development of the PVP was related to the incoming data from cortical regions receiving input from the relatively mature VHP. Therefore, we predicted that the microstructure of the PVP would be more similar to the VHP that precedes it than to the DHP that follows it. Because this prediction was related to how the white matter develops, we expected to find these results in the child sample, but not in the adult sample. Results were in line with our predictions. The PVP clustered with the VHP pathway in the child sample but not in the adult sample (**Figure 5c**). Finding that PVP and VHP tracts are clustered together in the child sample but separately in the adult sample suggests that PVP and VHP pathways have a different relationship in childhood than in adulthood. Our interpretation of this result is that data

input received from a relatively mature pathway has a developmental effect on the receiving pathway, but only when the receiving pathway is undergoing active developmental change.

Our final analysis was designed to characterize the relationship between the PVP and literacy. The purpose of this analysis was, first, to demonstrate that PVP development is relatable to behavior and, second, to contribute to our understanding of the nature of information communicated along PVP tracts. We found that FA in the posterior arcuate (pArc) that connects posterior ventral temporal cortex and inferior parietal lobe predicted children's visual-motor integration composite scores and, more specifically, predicted performance on the visual perception subtask. We found no other behavioral associations with any other white matter pathway tested (**Analysis 3.2**), suggesting some degree of specificity to the pArc and visual-motor skill. Our results suggest that the anatomical connectivity between the posterior ventral-temporal cortex and inferior parietal lobe may be related to the development of the visual perceptual aspect of visual-motor integration.

Many studies have found a relationship between the pArc and literacy in children 7 years and older (26–32). Yet we did not find a similar association. Instead, we found an association between the left pArc and the perceptual aspect of visual-motor skill (**Analysis 3.1**). We attribute the apparent discrepancy between our results and the majority of the prior work to differences in the age range of the child samples used in our study and prior work. All but one prior study (83) used children 7 years and older while our sample was slightly younger, 5-8 year old children. The apparent discrepancy with the single study finding a relationship between pArc and literacy in the age range of our sample suggests that future work will be necessary to better understand the relationship between the pArc and literacy development. Indeed, a breadth of behavioral work has indicated that visual-motor skill development positively predicts literacy development in this age range (93–99), suggesting that the left pArc's relationship with visual-motor skill may be a precursor to its relationship with literacy.

Taken together, our results suggest a key role for the PVP in the development of the dorsal visual stream. Our main findings are that the microstructure in the PVP is (1) more adult-like than in the dorsal visual stream, (2) more similar to the microstructure of the ventral visual stream than the dorsal visual stream, and (3) predicted by performance on a perceptual matching task in children ages 5-8 years. We interpret these results to suggest that the development of the dorsal stream trails behind the development of the posterior vertical tracts in this age range and may be driven by input received through the PVP during learning. We extend this interpretation to understand the development of the PVP; PVP development trails behind ventral stream development and may be driven by input received through ventral stream tracts. These results and our interpretation are consistent with a large body of work that has demonstrated that sensory input is a major driver of developmental change in the brain (109–112) and support our input-driven model of white matter development: white matter develops earlier in tracts closer to sensory input and later in tracts further away from sensory input. We propose that this developmental trajectory is related, at least in part, to the feed-forward propagation of sensory information along the major white matter pathways (**Figure 1**).

References

1. M. A. Goodale, A. D. Milner, Separate visual pathways for perception and action. *Trends Neurosci.* **15**, 20–25 (1992).

2. A. D. Milner, M. A. Goodale, Two visual systems re-viewed. *Neuropsychologia* **46**, 774–785 (2008).

3. H. Takemura, *et al.*, A major human white matter pathway between dorsal and ventral visual cortex. *Cereb. Cortex* **26**, 2205–2214 (2015).

4. I. Sani, B. C. McPherson, H. Stemmann, F. Pestilli, W. A. Freiwald, Functionally defined white matter of the macaque monkey brain reveals a dorso-ventral attention network. *Elife* **8** (2019).

5. G. T. Saber, F. Pestilli, C. E. Curtis, Saccade planning evokes topographically specific activity in the dorsal and ventral streams. *J. Neurosci.* **35**, 245–252 (2015).

6. L. G. Ungerleider, J. V. Haxby, “What”and “where”in the human brain. *Curr. Opin. Neurobiol.* **4**, 157–165 (1994).

7. A. D. Milner, How do the two visual streams interact with each other? *Exp. Brain Res.* **235**, 1297–1308 (2017).

8. T. W. James, J. Culham, G. K. Humphrey, A. D. Milner, M. A. Goodale, Ventral occipital lesions impair object recognition but not object-directed grasping: an fMRI study. *Brain* **126**, 2463–2475 (2003).

9. M. Goodale, D. Milner, *Sight Unseen: An Exploration of Conscious and Unconscious Vision* (OUP Oxford, 2013).

10. K. H. James, G. K. Humphrey, M. A. Goodale, Manipulating and recognizing virtual objects: where the action is. *Can. J. Exp. Psychol.* **55**, 111–120 (2001).

11. J. C. Culham, *et al.*, Visually guided grasping produces fMRI activation in dorsal but not ventral stream brain areas. *Exp. Brain Res.* **153**, 180–189 (2003).

12. B. Z. Mahon, N. Kumar, J. Almeida, Spatial frequency tuning reveals interactions between the dorsal and ventral visual systems. *J. Cogn. Neurosci.* **25**, 862–871 (2013).

13. P. Janssen, B. E. Verhoef, E. Premereur, Functional interactions between the macaque dorsal and ventral visual pathways during three-dimensional object vision. *Cortex* (2018).

14. E. Freud, J. C. Culham, G. Namdar, M. Behrmann, Object complexity modulates the association between action and perception in childhood. *J. Exp. Child Psychol.* **179**, 56–72 (2019).

15. C. Hanisch, J. Konczak, C. Dohle, The effect of the Ebbinghaus illusion on grasping behaviour of children. *Exp. Brain Res.* **137**, 237–245 (2001).

16. M. Catani, D. K. Jones, D. H. Ffytche, Perisylvian language networks of the human brain. *Ann. Neurol.* **57**, 8–16 (2005).

17. K. S. Weiner, J. D. Yeatman, B. A. Wandell, The posterior arcuate fasciculus and the vertical occipital fasciculus. *Cortex* **97**, 274–276 (2017).

18. Y. Wu, D. Sun, Y. Wang, Y. Wang, Y. Wang, Tracing short connections of the temporo-parieto-occipital region in the human brain using diffusion spectrum imaging and fiber dissection. *Brain Res.* **1646**, 152–159 (2016).

19. A. Kamali, H. I. Sair, A. Radmanesh, K. M. Hasan, Decoding the superior parietal lobule connections of the

superior longitudinal fasciculus/arcuate fasciculus in the human brain. *Neuroscience* **277**, 577–583 (2014).

20. N. Makris, *et al.*, Delineation of the middle longitudinal fascicle in humans: a quantitative, in vivo, DT-MRI study. *Cereb. Cortex* **19**, 777–785 (2009).

21. N. Makris, *et al.*, Human middle longitudinal fascicle: segregation and behavioral-clinical implications of two distinct fiber connections linking temporal pole and superior temporal gyrus with the angular gyrus or superior parietal lobule using multi-tensor tractography. *Brain Imaging Behav.* **7**, 335–352 (2013).

22. N. Makris, *et al.*, Mapping temporo-parietal and temporo-occipital cortico-cortical connections of the human middle longitudinal fascicle in subject-specific, probabilistic, and stereotaxic Talairach spaces. *Brain Imaging Behav.* **11**, 1258–1277 (2017).

23. N. Menjot de Champfleur, *et al.*, Middle longitudinal fasciculus delineation within language pathways: A diffusion tensor imaging study in human. *Eur. J. Radiol.* **82**, 151–157 (2013).

24. I. L. Maldonado, *et al.*, Evidence of a middle longitudinal fasciculus in the human brain from fiber dissection. *J. Anat.* **223**, 38–45 (2013).

25. D. Bullock, *et al.*, Associative white matter connecting the dorsal and ventral posterior human cortex. *Brain Struct. Funct.* (2019) https:/doi.org/10.1007/s00429-019-01907-8.

26. G. K. Deutsch, *et al.*, Children's reading performance is correlated with white matter structure measured by diffusion tensor imaging. *Cortex* **41**, 354–363 (2005).

27. J. D. Yeatman, R. F. Dougherty, M. Ben-Shachar, B. A. Wandell, Development of white matter and reading skills. *Proc. Natl. Acad. Sci. U. S. A.* **109**, E3045–53 (2012).

28. J. D. Yeatman, *et al.*, Anatomical properties of the arcuate fasciculus predict phonological and reading skills in children. *J. Cogn. Neurosci.* **23**, 3304–3317 (2011).

29. B. A. Wandell, J. D. Yeatman, Biological development of reading circuits. *Curr. Opin. Neurobiol.* **23**, 261–268 (2013).

30. Y. Wang, *et al.*, Development of tract-specific white matter pathways during early reading development in at-risk children and typical controls. *Cereb. Cortex* **27**, 2469–2485 (2017).

31. E. Huber, P. M. Donnelly, A. Rokem, J. D. Yeatman, Rapid and widespread white matter plasticity during an intensive reading intervention. *Nat. Commun.* **9**, 2260 (2018).

32. T. Klingberg, *et al.*, Microstructure of temporo-parietal white matter as a basis for reading ability: evidence from diffusion tensor magnetic resonance imaging. *Neuron* **25**, 493–500 (2000).

33. C. Lebel, L. Walker, A. Leemans, L. Phillips, C. Beaulieu, Microstructural maturation of the human brain from childhood to adulthood. *Neuroimage* **40**, 1044–1055 (2008).

34. J. Stiles, N. Akshoomoff, F. Haist, "The development of visuospatial processing" in *Neural Circuit Development and Function in the Brain*, (Elsevier, 2013), pp. 271–296.

35. P. Klaver, V. Marcar, E. Martin, "Chapter 7 - Neurodevelopment of the visual system in typically developing children" in *Progress in Brain Research*, O. Braddick, J. Atkinson, G. M. Innocenti, Eds. (Elsevier, 2011), pp. 113–136.

36. T. Loenneker, *et al.*, Microstructural development: organizational differences of the fiber architecture between children and adults in dorsal and ventral visual streams. *Hum. Brain Mapp.* **32**, 935–946 (2011).

37. D. Bonekamp, *et al.*, Diffusion tensor imaging in children and adolescents: reproducibility, hemispheric, and

age-related differences. *Neuroimage* **34**, 733–742 (2007).

38. C. Pierpaoli, P. J. Basser, Toward a quantitative assessment of diffusion anisotropy. *Magn. Reson. Med.* **36**, 893–906 (1996).

39. J. D. Yeatman, R. F. Dougherty, N. J. Myall, B. A. Wandell, H. M. Feldman, Tract profiles of white matter properties: automating fiber-tract quantification. *PLoS One* **7**, e49790 (2012).

40. B. D. Peters, *et al.*, Age-related differences in white matter tract microstructure are associated with cognitive performance from childhood to adulthood. *Biol. Psychiatry* **75**, 248–256 (2014).

41. Y. Lerner, T. Hendler, D. Ben-Bashat, M. Harel, R. Malach, A hierarchical axis of object processing stages in the human visual cortex. *Cereb. Cortex* **11**, 287–297 (2001).

42. M. Riesenhuber, T. Poggio, Hierarchical models of object recognition in cortex. *Nat. Neurosci.* **2**, 1019–1025 (1999).

43. D. J. Felleman, D. C. Van Essen, Distributed hierarchical processing in the primate cerebral cortex. *Cereb. Cortex* **1**, 1–47 (1991).

44. J. Hegdé, D. J. Felleman, Reappraising the Functional Implications of the Primate Visual Anatomical Hierarchy. *Neuroscientist* **13**, 416–421 (2007).

45. T. Serre, A. Oliva, T. Poggio, A feedforward architecture accounts for rapid categorization. *Proc. Natl. Acad. Sci. U. S. A.* **104**, 6424–6429 (2007).

46. T. Poggio, S. Ullman, Vision: are models of object recognition catching up with the brain? *Ann. N. Y. Acad. Sci.* **1305**, 72–82 (2013).

47. H. Johansen-Berg, C. S. Baptista, A. G. Thomas, Human structural plasticity at record speed. *Neuron* **73**, 1058–1060 (2012).

48. C. Sampaio-Baptista, Z.-B. Sanders, H. Johansen-Berg, Structural Plasticity in Adulthood with Motor Learning and Stroke Rehabilitation. *Annu. Rev. Neurosci.* **41**, 25–40 (2018).

49. C. Sampaio-Baptista, *et al.*, Motor skill learning induces changes in white matter microstructure and myelination. *J. Neurosci.* **33**, 19499–19503 (2013).

50. S. L. Bengtsson, *et al.*, Extensive piano practicing has regionally specific effects on white matter development. *Nat. Neurosci.* **8**, 1148–1150 (2005).

51. D. N. P. Jeremy D. Schmahmann, *Fiber Pathways of the Brain* (Oxford University Press, 2006).

52. S. Uda, *et al.*, Normal development of human brain white matter from infancy to early adulthood: a diffusion tensor imaging study. *Dev. Neurosci.* **37**, 182–194 (2015).

53. J. E. Reynolds, M. N. Grohs, D. Dewey, C. Lebel, Global and regional white matter development in early childhood. *Neuroimage* **196**, 49–58 (2019).

54. S.-H. Choi, G. Jeong, Y.-B. Kim, Z.-H. Cho, Proposal for human visual pathway in the extrastriate cortex by fiber tracking method using diffusion-weighted MRI. *Neuroimage* **220**, 117145 (2020).

55. M. Mishkin, L. G. Ungerleider, K. A. Macko, Object vision and spatial vision: two cortical pathways. *Trends Neurosci.* **6**, 414–417 (1983).

56. G. Rizzolatti, M. Matelli, Two different streams form the dorsal visual system: anatomy and functions. *Exp.*

Brain Res. **153**, 146–157 (2003).

57. F. Binkofski, L. J. Buxbaum, Two action systems in the human brain. *Brain Lang.* **127**, 222–229 (2013).

58. M. Catani, D. K. Jones, R. Donato, D. H. Ffytche, Occipito-temporal connections in the human brain. *Brain* **126**, 2093–2107 (2003).

59. S. Mori, *et al.*, Imaging cortical association tracts in the human brain using diffusion-tensor-based axonal tracking. *Magnetic Resonance in Medicine: An Official Journal of the International Society for Magnetic Resonance in Medicine* **47**, 215–223 (2002).

60. S. S. Panesar, F.-C. Yeh, T. Jacquesson, W. Hula, J. C. Fernandez-Miranda, A Quantitative Tractography Study Into the Connectivity, Segmentation and Laterality of the Human Inferior Longitudinal Fasciculus. *Front. Neuroanat.* **12**, 47 (2018).

61. R. J. Tusa, L. G. Ungerleider, The inferior longitudinal fasciculus: a reexamination in humans and monkeys. *Ann. Neurol.* **18**, 583–591 (1985).

62. F. Latini, *et al.*, Segmentation of the inferior longitudinal fasciculus in the human brain: A white matter dissection and diffusion tensor tractography study. *Brain Res.* **1675**, 102–115 (2017).

63. M. Catani, R. J. Howard, S. Pajevic, D. K. Jones, Virtual in vivo interactive dissection of white matter fasciculi in the human brain. *Neuroimage* **17**, 77–94 (2002).

64. I. N. C. Lawes, *et al.*, Atlas-based segmentation of white matter tracts of the human brain using diffusion tensor tractography and comparison with classical dissection. *Neuroimage* **39**, 62–79 (2008).

65. S. Mori, *et al.*, Stereotaxic white matter atlas based on diffusion tensor imaging in an ICBM template. *Neuroimage* **40**, 570–582 (2008).

66. E. Ortibus, *et al.*, Integrity of the inferior longitudinal fasciculus and impaired object recognition in children: a diffusion tensor imaging study. *Dev. Med. Child Neurol.* **54**, 38–43 (2012).

67. J. D. Yeatman, *et al.*, The vertical occipital fasciculus: a century of controversy resolved by in vivo measurements. *Proc. Natl. Acad. Sci. U. S. A.* **111**, E5214–23 (2014).

68. H. Takemura, F. Pestilli, K. S. Weiner, Comparative neuroanatomy: Integrating classic and modern methods to understand association fibers connecting dorsal and ventral visual cortex. *Neurosci. Res.* **146**, 1–12 (2019).

69. T. Kaneko, *et al.*, Spatial organization of occipital white matter tracts in the common marmoset. *Brain Struct. Funct.* **225**, 1313–1326 (2020).

70. G. Golarai, *et al.*, Differential development of high-level visual cortex correlates with category-specific recognition memory. *Nat. Neurosci.* **10**, 512–522 (2007).

71. K. S. Scherf, M. Behrmann, K. Humphreys, B. Luna, Visual category-selectivity for faces, places and objects emerges along different developmental trajectories. *Dev. Sci.* **10**, F15–F30 (2007).

72. T. Dekker, D. Mareschal, M. I. Sereno, M. H. Johnson, Dorsal and ventral stream activation and object recognition performance in school-age children. *Neuroimage* **57**, 659–670 (2011).

73. K. H. James, A. J. Kersey, Dorsal stream function in the young child: an fMRI investigation of visually guided action. *Dev. Sci.* **21** (2018).

74. P. Avesani, *et al.*, The open diffusion data derivatives, brain data upcycling via integrated publishing of

derivatives and reproducible open cloud services. *Sci Data* **6**, 69 (2019).

75. S. Hayashi, B. McPherson, B. Caron, *HCP ACPC Alignment (T1)* (brainlife.io, 2018) https:/doi.org/10.25663/BL.APP.99.

76. B. McPherson, *mrtrix3 preprocess* (brainlife.io, 2018) https:/doi.org/10.25663/BL.APP.68.

77. P. J. Basser, J. Mattiello, D. LeBihan, MR diffusion tensor spectroscopy and imaging. *Biophys. J.* **66**, 259–267 (1994).

78. B. McPherson, *mrtrix3 act* (brainlife.io, 2018) https:/doi.org/10.25663/BL.APP.101.

79. D. Bullock, *White Matter Anatomy Segmentation* (brainlife.io, 2019) https:/doi.org/10.25663/BRAINLIFE.APP.188.

80. B. Caron, *Tract Analysis Profiles* (brainlife.io, 2019) https:/doi.org/10.25663/BRAINLIFE.APP.185.

81. F. Pestilli, J. D. Yeatman, A. Rokem, K. N. Kay, B. A. Wandell, Evaluation and statistical inference for human connectomes. *Nat. Methods* **11**, 1058–1063 (2014).

82. I. Broce, B. Bernal, N. Altman, P. Tremblay, A. S. Dick, Fiber tracking of the frontal aslant tract and subcomponents of the arcuate fasciculus in 5–8-year-olds: Relation to speech and language function. *Brain Lang.* **149**, 66–76 (2015).

83. I. J. Broce, *et al.*, Fiber pathways supporting early literacy development in 5–8-year-old children. *Brain Cogn.* **134**, 80–89 (2019).

84. G. A. F. Seber, *Multivariate Observations* (John Wiley & Sons, 2009).

85. M. A. A. Cox, T. F. Cox, “Multidimensional Scaling” in *Handbook of Data Visualization*, C.-H. Chen, W. Härdle, A. Unwin, Eds. (Springer Berlin Heidelberg, 2008), pp. 315–347.

86. W. S. Torgerson, Multidimensional scaling: I. Theory and method. *Psychometrika* **17**, 401–419 (1952).

87. J. B. Kruskal, NONMETRIC MULTIDIMENSIONAL SCALING: A NUMERICAL METHOD. *Psychometrika* **29**, 115–129 (1964).

88. I. W. Eisenberg, *et al.*, Uncovering the structure of self-regulation through data-driven ontology discovery. *Nat. Commun.* **10**, 2319 (2019).

89. D. Arthur, S. Vassilvitskii, k-means++: The Advantages of Careful Seeding (2006) (August 14, 2020).

90. R. B. Cattell, The Scree Test For The Number Of Factors. *Multivariate Behav. Res.* **1**, 245–276 (1966).

91. L. Kaufman, P. J. Rousseeuw, *Finding Groups in Data: An Introduction to Cluster Analysis* (John Wiley & Sons, 2009).

92. E. Moulton, *et al.*, Connectivity between the visual word form area and the parietal lobe improves after the first year of reading instruction: a longitudinal MRI study in children. *Brain Struct. Funct.* **224**, 1519–1536 (2019).

93. C. E. Cameron, *et al.*, Fine motor skills and executive function both contribute to kindergarten achievement. *Child Dev.* **83**, 1229–1244 (2012).

94. A. G. Carlson, E. Rowe, T. W. Curby, Disentangling fine motor skills’ relations to academic achievement: the relative contributions of visual-spatial integration and visual-motor coordination. *J. Genet. Psychol.* **174**,

514–533 (2013).

95. D. Grissmer, K. J. Grimm, S. M. Aiyer, W. M. Murrah, J. S. Steele, Fine motor skills and early comprehension of the world: two new school readiness indicators. *Dev. Psychol.* **46**, 1008–1017 (2010).

96. L. H. Dinehart, Handwriting in early childhood education: Current research and future implications. *Journal of Early Childhood Literacy* **15**, 97–118 (2015).

97. G. J. Clark, The relationship between handwriting, reading, fine motor and visual-motor skills in kindergarteners (2010).

98. N. E. Fears, J. J. Lockman, How beginning handwriting is influenced by letter knowledge: Visual--motor coordination during children's form copying. *J. Exp. Child Psychol.* **171**, 55–70 (2018).

99. J. E. Maldarelli, B. A. Kahrs, S. C. Hunt, J. J. Lockman, Development of early handwriting: Visual-motor control during letter copying. *Dev. Psychol.* **51**, 879–888 (2015).

100. C. Lebel, S. Treit, C. Beaulieu, A review of diffusion MRI of typical white matter development from early childhood to young adulthood. *NMR Biomed.* **32**, e3778 (2019).

101. H. Huang, L. Vasung, Gaining insight of fetal brain development with diffusion MRI and histology. *Int. J. Dev. Neurosci.* **32**, 11–22 (2014).

102. J. Dubois, *et al.*, The early development of brain white matter: a review of imaging studies in fetuses, newborns and infants. *Neuroscience* **276**, 48–71 (2014).

103. A. Qiu, S. Mori, M. I. Miller, Diffusion tensor imaging for understanding brain development in early life. *Annu. Rev. Psychol.* **66**, 853–876 (2015).

104. C. Lebel, S. Deoni, The development of brain white matter microstructure. *Neuroimage* **182**, 207–218 (2018).

105. S. Wang, K. M. Young, White matter plasticity in adulthood. *Neuroscience* **276**, 148–160 (2014).

106. Y. Assaf, O. Pasternak, Diffusion tensor imaging (DTI)-based white matter mapping in brain research: a review. *J. Mol. Neurosci.* **34**, 51–61 (2008).

107. M. Moseley, Diffusion tensor imaging and aging--a review. *NMR in Biomedicine: An International Journal Devoted to the Development and Application of Magnetic Resonance In Vivo* **15**, 553–560 (2002).

108. M. Thiebaut de Schotten, C. Foulon, P. Nachev, Brain disconnections link structural connectivity with function and behaviour. *Nat. Commun.* **11**, 5094 (2020).

109. A. Meyer, Paul Flechsig's System of Myelogenetic Cortical Localization in the Light of Recent Research in Neuroanatomy and Neurophysiology Part I. *Can. J. Neurol. Sci.* **8**, 1–6 (1981).

110. A. Meyer, Paul Flechsig's System of Myelogenetic Cortical Localization In the Light of Recent Research in Neuroanatomy and Neurophysiology Part II. *Can. J. Neurol. Sci.* **8**, 95–104 (1981).

111. P. Flechsig Of Leipsic, DEVELOPMENTAL (MYELOGENETIC) LOCALISATION OF THE CEREBRAL CORTEX IN THE HUMAN SUBJECT. *Lancet* **158**, 1027–1030 (1901).

112. D. Maurer, T. L. Lewis, Visual systems. *The Neurobiology of Brain and Behavioral* (2018).

113. K. E. Beery, Beery VMI: The Beery-Buktenica developmental test of visual-motor integration. *Minneapolis, MN: Pearson* (2004).

114. C. G. Matthews, H. Klove, Instruction manual for the adult neuropsychology test battery. *Madison, WI: University of Wisconsin Medical School* **36** (1964).

115. B. Merker, K. Podell, “Grooved Pegboard Test” in *Encyclopedia of Clinical Neuropsychology*, J. S. Kreutzer, J. DeLuca, B. Caplan, Eds. (Springer New York, 2011), pp. 1176–1178.

116. F. A. Schrank, B. J. Wendling, The Woodcock--Johnson IV. *Contemporary Intellectual Assessment: Theories, Tests, and Issues*, 383 (2018).

117. M. F. Glasser, *et al.*, The minimal preprocessing pipelines for the Human Connectome Project. *Neuroimage* **80**, 105–124 (2013).

118. V. Fonov, *et al.*, Unbiased average age-appropriate atlases for pediatric studies. *Neuroimage* **54**, 313–327 (2011).

119. B. Fischl, FreeSurfer. *Neuroimage* **62**, 774–781 (2012).

120. S. Hayashi, L. Kitchell, F. Pestilli, *Freesurfer* (brainlife.io, 2017) https:/doi.org/10.25663/BL.APP.0.

121. C. Destrieux, B. Fischl, A. Dale, E. Halgren, Automatic parcellation of human cortical gyri and sulci using standard anatomical nomenclature. *Neuroimage* **53**, 1–15 (2010).

122. B. Caron, *FSL Top-up & Eddy - CUDA* https:/doi.org/10.25663/brainlife.app.287.

123. B. Ades-Aron, *et al.*, Evaluation of the accuracy and precision of the diffusion parameter EStImation with Gibbs and NoisE removal pipeline. *Neuroimage* **183**, 532–543 (2018).

124. D. N. Greve, B. Fischl, Accurate and robust brain image alignment using boundary-based registration. *Neuroimage* **48**, 63–72 (2009).

125. J.-D. Tournier, F. Calamante, A. Connelly, MRtrix: Diffusion tractography in crossing fiber regions. *Int. J. Imaging Syst. Technol.* **22**, 53–66 (2012).

126. J.-D. Tournier, F. Calamante, A. Connelly, Robust determination of the fibre orientation distribution in diffusion MRI: non-negativity constrained super-resolved spherical deconvolution. *Neuroimage* **35**, 1459–1472 (2007).

127. R. E. Smith, J.-D. Tournier, F. Calamante, A. Connelly, Anatomically-constrained tractography: improved diffusion MRI streamlines tractography through effective use of anatomical information. *Neuroimage* **62**, 1924–1938 (2012).

128. H. Takemura, C. F. Caiafa, B. A. Wandell, F. Pestilli, Ensemble Tractography. *PLoS Comput. Biol.* **12**, e1004692 (2016).

129. D. Wassermann, *et al.*, The white matter query language: a novel approach for describing human white matter anatomy. *Brain Struct. Funct.* **221**, 4705–4721 (2016).

130. D. Wassermann, *et al.*, On describing human white matter anatomy: the white matter query language. *Med. Image Comput. Comput. Assist. Interv.* **16**, 647–654 (2013).

131. D. Bullock, *Remove Tract Outliers (new wmc input/output)* (brainlife.io, 2019) https:/doi.org/10.25663/BRAINLIFE.APP.195.

132. M. T. de Schotten, *et al.*, A lateralized brain network for visuospatial attention. *Nat. Neurosci.* **14**, 1245 (2011).

133. A. Rokem, *et al.*, The visual white matter: The application of diffusion MRI and fiber tractography to vision

science. *J. Vis.* **17**, 4 (2017).

134. A. Kamali, A. E. Flanders, J. Brody, J. V. Hunter, K. M. Hasan, Tracing superior longitudinal fasciculus connectivity in the human brain using high resolution diffusion tensor tractography. *Brain Struct. Funct.* **219**, 269–281 (2014).

135. A. S. Dick, D. Garic, P. Graziano, P. Tremblay, The frontal aslant tract (FAT) and its role in speech, language and executive function. *Cortex* **111**, 148–163 (2019).